sciendo **Transactions on Aerospace Research** eISSN 2545-2835, VOL. 268, NO. 3/2022, 56-74
DOI: 10.2478/tar-2022-0017

DETERMINATION OF THE GEOMETRIC PROPERTIES OF A JET ENGINE FAN BLADES BASED ON MODAL VIBRATION TESTING

Maciej Osiewicz[1]*, **Sławomir Cieślak**[1], **Marcin Bielecki**[2]
[1] Łukasiewicz Research Network – Institute of Aviation, al. Krakowska 110/114, 02-256 Warsaw, Poland
[2] Baker Hughes Poland, al. Krakowska 110/114, 02-256 Warsaw, Poland

Abstract

The article presents an experimental method of determining the geometric properties of jet engine rotor airfoils based on modal vibration testing. The procedure is based on adjusting the results of analytical calculations to the laboratory outcomes. Experimental tests were carried out on a set of 20 jet engine fan blades made of AL7022-T6 aluminium alloy. Each blade differed in weight and geometric dimensions within the accepted design tolerance. Numerical analysis of five airfoils that differed in thickness was performed. Modal vibration test results were summarised and compared with the results obtained by the numerical method. The comparison revealed a high similarity of the frequency and form of vibrations acquired by numerical simulation for each of the blades in relation to the executed vibration testing. Based on the verification of the theoretical model with the results obtained through experimental testing, conclusions were drawn about the object's dynamic behaviour and its technological quality and geometric properties, whereby each of airfoil was probably thinned.

Keywords: blade vibration; modal analysis; finite elements; design; aviation
Type of the work: research article

1. INTRODUCTION

The fatigue process of materials under the influence of a long-term alternating load is a significant problem in modern technology. In the context of jet engines, both compressor and turbine blades are particularly vulnerable to this type of phenomenon, which may therefore result in the premature wear of those parts. The blade of an aircraft engine operates in very difficult conditions under the influence of high rotational speeds, pressures and temperatures [1]. According to the loads acting on them, they are subjected to extension, bending and torsional states [2,3]. Periodically changing stresses shorten the service life of structural elements because their destruction may occur at a value lower than the ultimate stress of the material. The result of this phenomenon is that a given material can undergo only a finite number of cycles [4,5]. The number depends on the load under which the material works, and with the increase in amplitude of the alternating stress, the number of cycles to failure decreases. For evaluation of the limit number of cycles that a given blade can operate, the applied stress-to-number of cycles to failure (S–N) fatigue curve—namely, the Wohler diagram—is used (Fig. 1). It can be divided into four sections describing the quasi-static problems, low-cycle fatigue (LCF), high-cycle fatigue (HCF) and permanent strength [6]. For HCF, only the Goodman–Soderberg fatigue curve is used. It helps to describe the permissible static-to-alternating stress ratio. It is widely used in relation to resonance vibrations [7].

* Corresponding Author: Maciej.Osiewicz@ilot.lukasiewicz.gov.pl
ARTICLE HISTORY **Received** 2022-01-26 **Revised** 2022-03-18 **Accepted** 2022-06-20

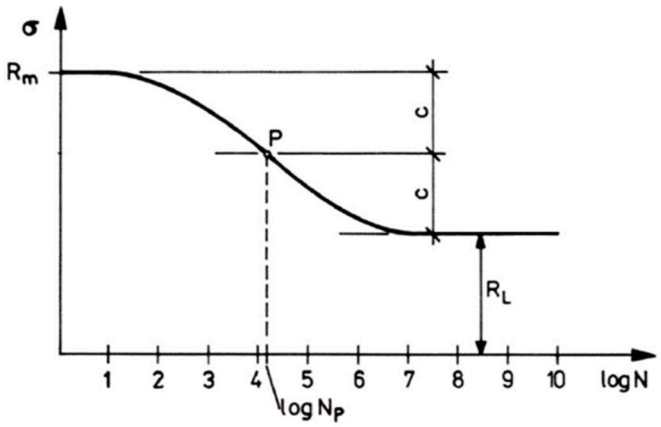

Figure 1. Wöhler curve for ferritic–pearlitic mild steel.
It is created by approximating the 50% probability of the concentration of fatigue test results for individual material stress levels and the number of load cycles until the crack occurs [6].

Resonance occurs when the natural frequency of a device, or its component, is at the same level as the frequency of the exciting force. To minimise the risk of overlapping frequencies, it is essential to determine the dynamic properties of the tested object. To fulfil this requirement, modal vibration analysis is used.

Modal analysis allows for description of the dynamic state of an object. It is also used as a non-destructive method for the diagnosis of wear of mechanical components, detection of damage [8–10], outlining the symptoms of blade cracking [11], or quality check (geometrical dimensions, and material-related or initial damages). The result is an ordered set of natural frequencies and modes, together with the corresponding damping coefficients [12], which indirectly can be used to analyse the material parameters [6]. The process of examining an object may take one of two ways, i.e., through an analytical description of the quantities characterising the dynamics of the system or by using a modal test on a real object.

The modal test of a real object is the most frequently used method of dynamic verification under all boundary conditions. Among the experimental methods, the most widely used are those using the impulse test [13], excitation with a sinusoidal signal in a given frequency band (sine sweep vibration testing) [14] and operational modal analysis, which is carried out by measuring vibrations during the operation of a machine or an object [15]. An alternative to the physical test on a real object is numerical analysis. It allows for determination of the frequencies and modes of natural vibrations of elements under various operating conditions, already at the design stage. The problem is the need for validation of the obtained results.

Modal analysis is widely used in the automotive, aviation [16–20], space [21] and construction [22] industries.

2. EXPERIMENTAL TEST RESEARCH

All the tests described in this chapter were carried out at the Materials and Structures Research Center, which is part of the Łukasiewicz Research Network–Institute of Aviation. The aim of the conducted tests was to determine the frequency and form of natural vibrations of the boundary layer ingestion-based propulsion fan blades. The impulse method was used for the tests. The experiment was carried out in the range of 0–2,000 Hz, which was the expected resonance range determined using the Campbell vibration diagram. A PCB Piezotronics company modal hammer with a PCB-086C01 model was used

to excite the tested objects with a force impulse, while the measurements were carried out using a microphone, two triaxial sensors, nine uniaxial sensors and a multichannel recorder. The experiment was performed on 20 rotor blades, made of aluminium alloy Al7022-T6, marked successively with numbers in the range of 01–20. Each of them slightly differed in mass and geometry within the design tolerance. The first step of the tests was to capture the free-vibration-mode shapes of one blade. Afterwards, measurements of the natural frequencies of all 20 blades were performed.

2.1. Measurement of the natural-vibration-mode shapes

Determination of the natural-vibration-mode shapes was carried out using a modal hammer, a microphone and 11 accelerometers glued to blade number 01 (measuring points with sensors attached are shown in Fig. 2). The sensors were connected to the recorder. The measurement points were assigned to the geometric model in which the airfoil was treated as untwisted (it was assumed that all sensors are placed in the same plane). The location of the accelerometers is presented in the "LMS Test.Lab: Impact Testing" system, used to visualise the mode of free vibrations of the tested elements (Fig. 3a).

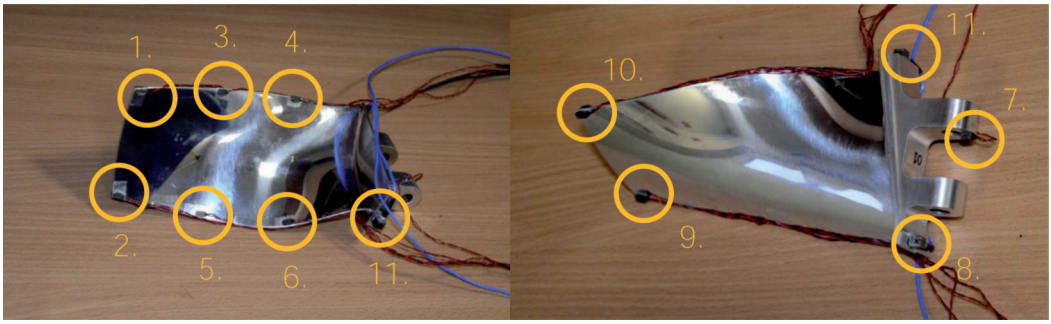

Figure 2. Location of sensors on airfoil no. 01.

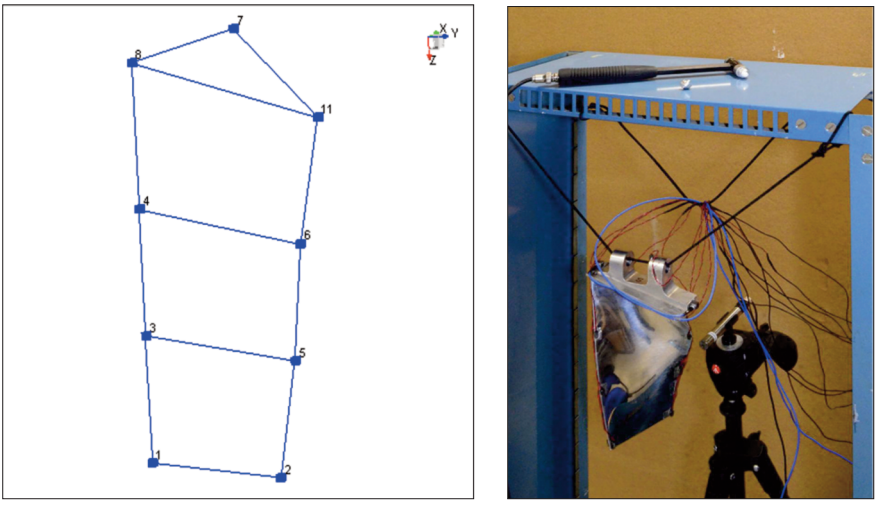

a) b)

Figure 3. a) grid drawn in the "LMS Test.Lab: Impact Testing" system; b) Blade with a set of sensors and a set up microphone during the tests (suspended on rubber tie rods).

During the first test, the object was suspended on a thin rubber string, and during the second one, on a braided cord. Both tests were performed under unsupported boundary conditions to obtain an unambiguous representation of the same state (i.e., 'free–free' condition) in numerical analysis. In order to eliminate damping during the measurements, the vibration damping time of the blade suspended on ties made of various materials was checked. Using the half-power method, a lower value was obtained for the braided cord blade set-up (Fig. 4); therefore, it was used in subsequent tests (Fig. 3b).

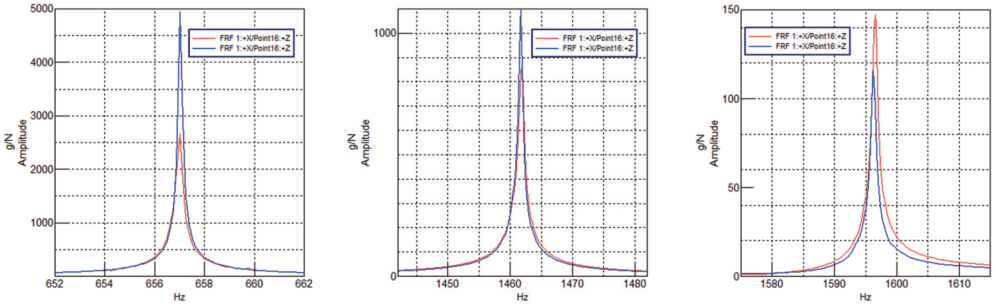

Figure 4. The acceleration spectrum of the first three vibration modes recorded by a sensor for an object suspended on a rubber string (red) and a braid (blue). Visible difference in the damping coefficient for the blade suspended on ties made of various materials while maintaining a constant natural frequency. FRF, frequency response function.

The measurement was made by excitation of the suspended blade with a force impulse and simultaneous registration of the response spectrum using acceleration sensors. Moreover, the signal measured with the microphone was also recorded during the test. This was done to compare the frequency of the emitted sound with the response recorded by the accelerometers.

2.2. Results of the natural-vibration-mode shape measurement

In the analysed frequency range, three modes of free vibrations (two bending and one torsional modes) were identified. They occurred at the frequencies of 647.25 Hz, 1,435 Hz and 1,694 Hz, respectively. The movements of the elements of each blade are shown in Fig. 5.

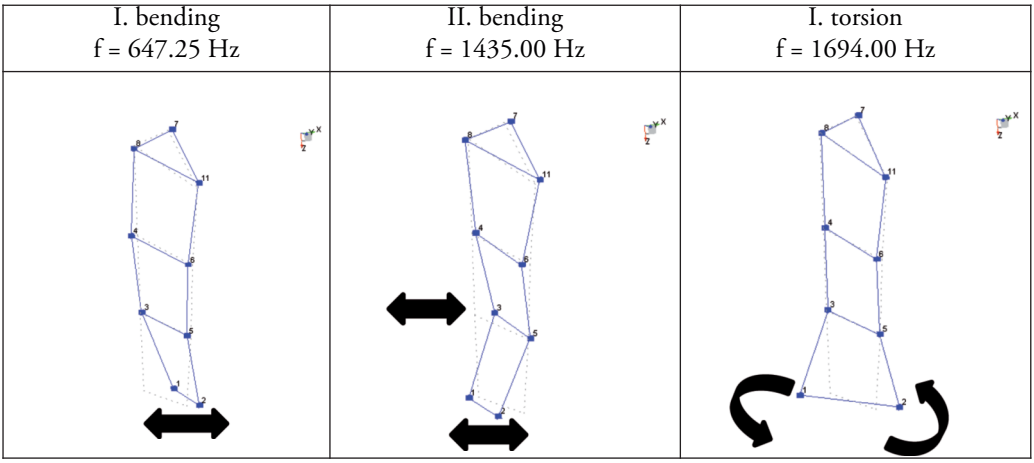

Figure 5. Registered modes of free vibrations of blade no. 01 presented in the LMS programme.

2.3. Measurement of natural frequency

During measurement of the natural frequency, two types of sensors were used to compare the obtained results. The study was carried out using an accelerometer and a microphone. For blades 01 and 02, the accelerometer was glued at the apex near the leading edge (see Fig. 7). This position was the result of an earlier study, presented in chapter 2.2, in which the greatest mixing of each of the mode shapes was recorded at this point. Then, as before, the objects were attached to te ωndons and excited by a force impulse. The results of the test are presented in Table 1. Moreover, the amplitude–frequency characteristics obtained by measuring with an accelerometer and a microphone for the first three vibration frequencies are shown on Fig. 8. The damping factor for each mode was calculated using the 'half-power (or 3 dB) method' based on the formula on frequency response functions (FRFs) [23]:

$$\zeta = \frac{1}{2Q} \cdot \frac{\Delta\omega_{3dB}}{2\omega_0},$$

where ω_0 – is the frequency at the peak response, and $\Delta\omega_{3dB}$ is the difference between the left '1' and right '2' frequencies, where the response is 3 dB lower than the peak response (Fig. 6).

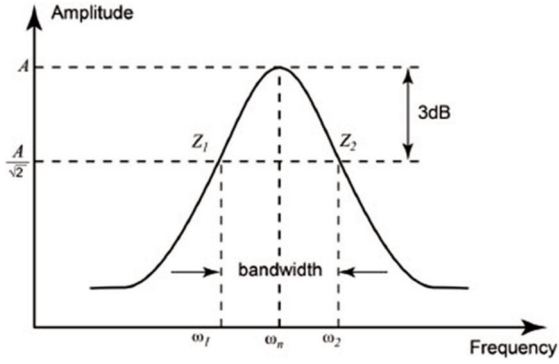

Figure 6. Half-power band method [22].

Figure 7. Blade with an attached acceleration sensor at the leading edge (marked with a yellow circle).

Table 1. Measurement of the blade vibration frequency using one acceleration sensor and a microphone.

Blade no. / measurement method	I. Bending	II. Bending	I. Torsion
01/microphone	660.5 Hz	1,469.6 Hz	1,600.5 Hz
01/sensor	660.5 Hz	1,469.6 Hz	1,600.5 Hz
02/microphone	657.1 Hz	1,462.0 Hz	1,596.5 Hz
02/sensor	657.1 Hz	1,462.0 Hz	1,596.5 Hz

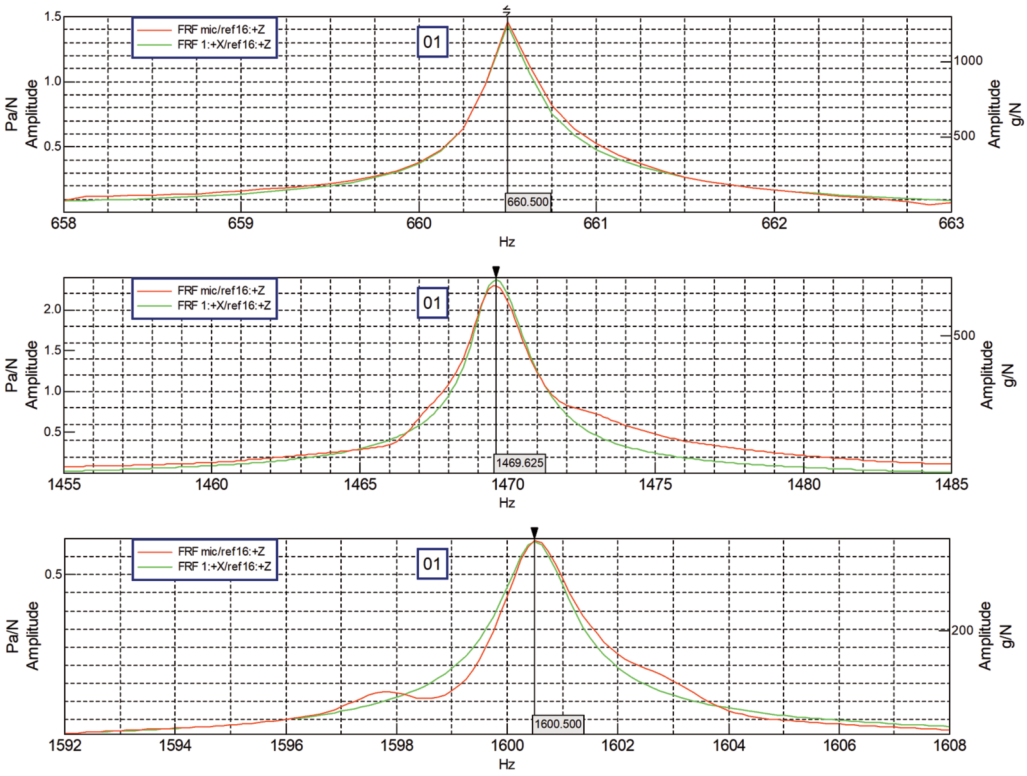

Figure 8. The amplitude–frequency characteristic from the indications of the microphone (red) and the acceleration sensor (green) for blade number 01 and the first three forms of vibration. FRF, frequency response function.

Later in the article, for the figures whose vertex was not sharp, the attenuation for the 'predicted'" peak was calculated based on the intersection of the extended straight lines running through the available adjacent points on the graph.

Measurement of the natural frequencies of two blades showed that the tests using an accelerometer or a microphone gave identical results. Therefore, it was decided that the remaining tests would be carried out without the use of acceleration sensors. This decision allowed for the reduction of interference caused by the sensors' mass and reduced the influence of the cables on the stiffness and damping of the entire system. As the result of previous tests, this configuration was used for the remaining experiments (measurement using the microphone only).

The results of the frequencies and damping coefficient obtained for each of the blade are presented in Table 2, based on which the graphs shown in Fig. 12 were created. They show the dependence of the obtained vibration frequency as a function of the mass of the tested object. The trend of the results does not meet common sense expectations because, as the mass of the blades increased, their frequency increased as well. Therefore, a hypothesis was adopted that the increase in mass was caused by the thickening of the airfoil, which had an indirect effect on the increase in structural stiffness. Verification of the validity of this hypothesis is the subject of the numerical analysis described later in the study. Moreover, Figs 9–11 show the amplitude–frequency characteristics for all tested objects, depending on the mode of natural vibrations.

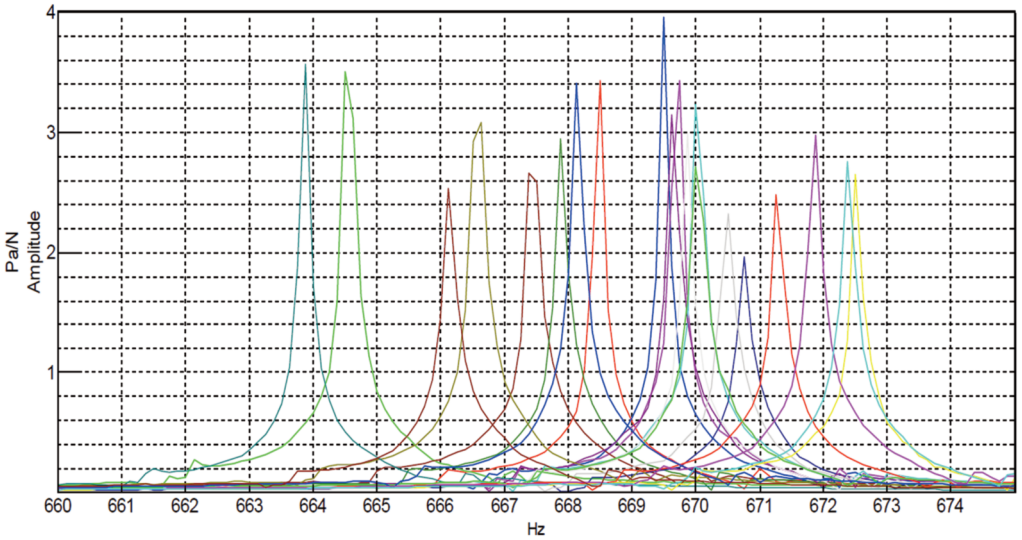

Figure 9. The amplitude–frequency characteristic for blade numbers 01–20 (vibration form I).

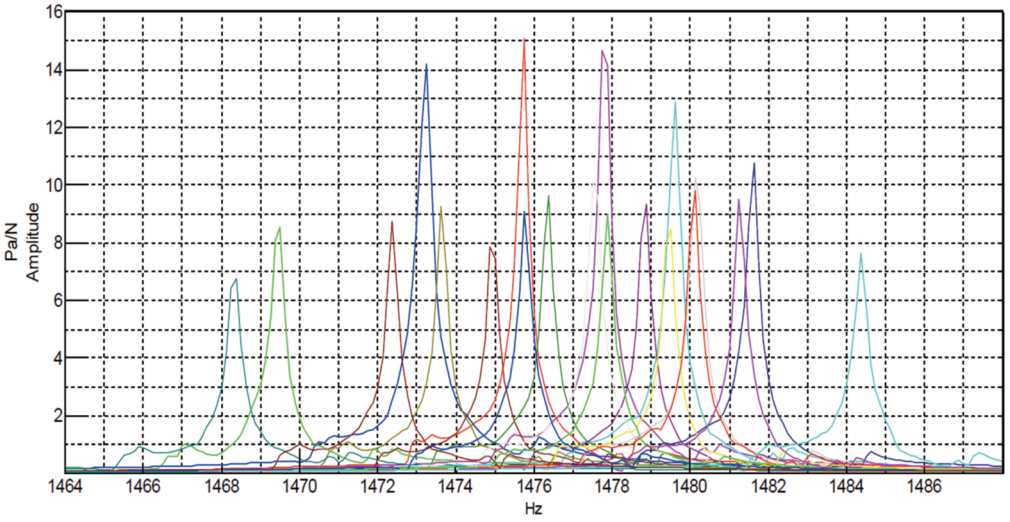

Figure 10. Amplitude–frequency characteristic for blade numbers 01–20 (vibration form II).

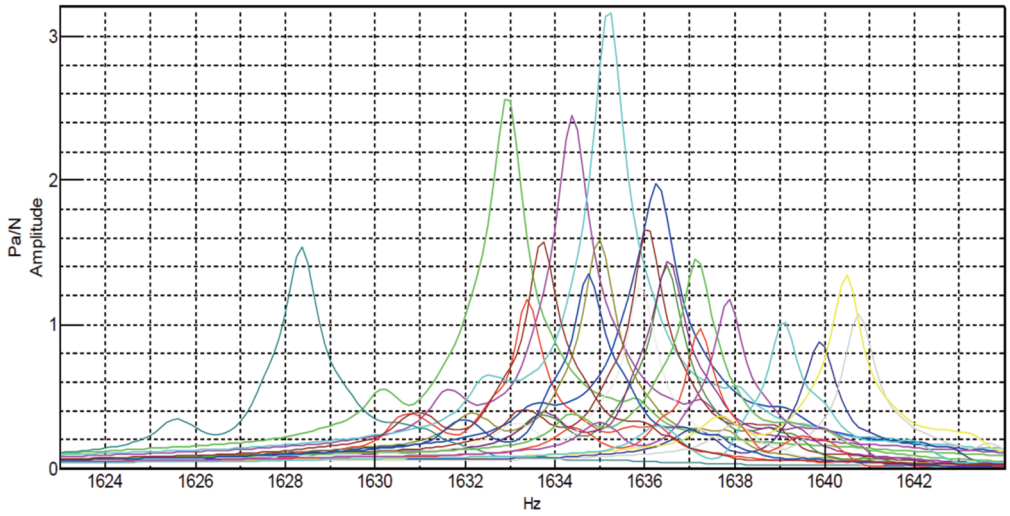

Figure 11. Amplitude–frequency characteristic for blade numbers 01–20 (vibration form III).

Table 2. Results of the measurements of the natural frequencies and the damping coefficients for all blades (values whose vertex was not a sharp interpolation of the peak prediction based on the intersection of the extended lines was performed), coefficient Q is non-dimensional.

Airfoil No.	I mode shape			II mode shape			III mode shape			mass
	f [Hz]	ζ %	Q	f [Hz]	ζ %	Q	f [Hz]	ζ %	Q	m [g]
1	668.5	0,011	4,420	1,475.75	0.008	6,353	1,633.38	0.018	2,839	417.1
2	664.5	0,012	4,344	1,469.5	0.008	5,977	1,632.88	0.022	2,289	414.6
3	669.5	0,010	4,934	1,473.25	0.010	4,874	1,636.25	0.027	1,863	413.1
4	669.75	0,014	3,703	1,477.75	0.008	6,191	1,634.38	0.022	2,269	417.3
5	670	0,015	3,435	1,479.63	0.009	5,427	1,635.25	0.021	2,342	417.4
6	667.375	0,014	3,647	1,474.88	0.008	6,433	1,636	0.020	2,449	414.8
7	667.875	0,013	3,883	1,476.38	0.009	5,778	1,636.5	0.020	2,550	415.6
8	670.75	0,015	3,336	1,481.63	0.009	5,444	1,639.88	0.020	2,533	418.1
9	669.625	0,014	3,513	1,478.88	0.008	6,043	1,636.5	0.023	2,212	417.9
10	666.625	0,015	3,367	1,473.63	0.009	5,831	1,635	0.020	2,448	414.5
11	663.875	0,011	4,494	1,468.38	0.009	5,868	1,628.38	0.021	2,343	413.7
12	669.875	0,012	4,296	1,477.5	0.009	5,856	1,635.88	0.019	2,598	414.6
13	670.5	0,015	3,238	1,480.13	0.008	6,038	1,640.75	0.018	2,753	417.4
14	672.5	0,014	3,456	1,479.5	0.008	6,003	1,640.5	0.019	2,600	413.5
15	671.25	0,016	3,155	1,480.13	0.009	5,557	1,637.25	0.016	3,046	415.4

Airfoil No.	I mode shape			II mode shape			III mode shape			mass
16	670	0,017	3,005	1,477.88	0.010	5,237	1,637.13	0.021	2,338	416.2
17	668.125	0,013	3,722	1,475.75	0.009	5,417	1,634.75	0.021	2,400	417.4
18	671.875	0,015	3,278	1,481.25	0.009	5,477	1,637.88	0.019	2,654	416.3
19	672.375	0,015	3,371	1,484.38	0.010	4,994	1,639.13	0.020	2,527	419.5
20	666.125	0,014	3,555	1,472.38	0.009	5,675	1,633.75	0.020	2,461	415.7

Average values of:								
I mode shape			II mode shape			III mode shape		
f [Hz]	ζ %	Q	f [Hz]	ζ %	Q	f [Hz]	ζ %	Q
669.05	0.014	3,708	1,476.93	0.009	5,724	1,636.07	0.020	2,476
Standard deviation of:								
I mode shape			II mode shape			III mode shape		
f [Hz]	ζ %	Q	f [Hz]	ζ %	Q	f [Hz]	ζ %	Q
2.42	0.002	522.6	4.08	0.001	420.2	2.90	0.002	250.4
Coefficient of variation for frequencies	0.4%		Coefficient of variation for frequencies	0.3%		Coefficient of variation for frequencies	0.2%	

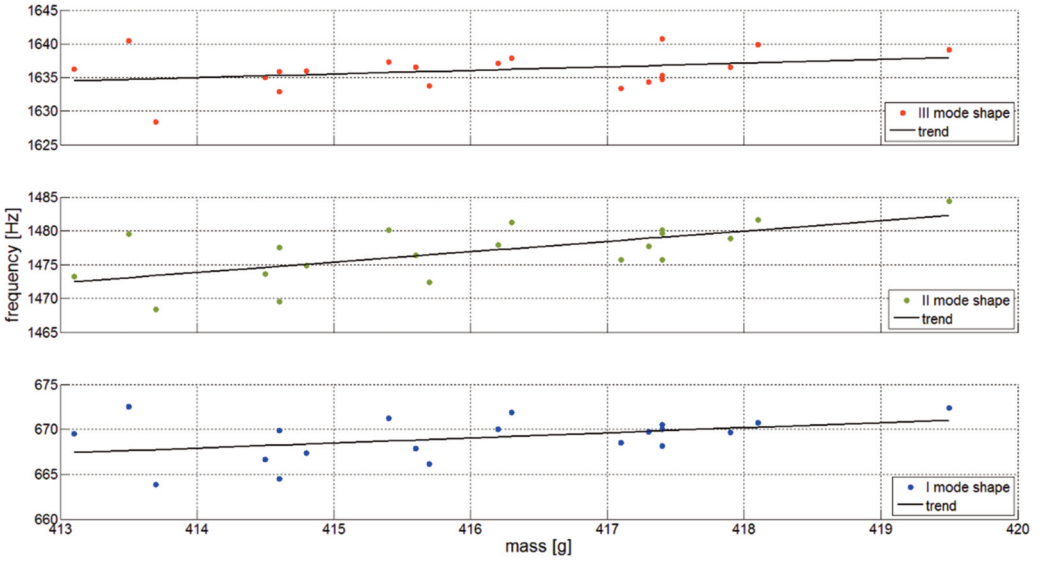

Figure 12. Influence of the change in blade mass on the obtained natural frequencies for each tested form.

3. NUMERICAL MODAL ANALYSIS

Numerical modal analysis allows the determination of the frequencies and mode shapes of free vibrations of tested objects already at the design stage, using the computer-aided design (CAD) model. The calculations were performed using ANSYS 19.2 in the 'Modal Analysis' module at the Aircraft Propulsion Department, which is part of the Łukasiewicz Research Network–Institute of Aviation. The numerical calculation process is divided into three steps, i.e., pre-processing (preparation of geometry for analysis), solver (calculations) and postprocessing (analysis of the obtained results).

3.1. Preparation of the model for analysis

The first stage of numerical calculations was to adopt parameters that best reflect the properties of the material from which the blades were made. An ideally elastic material model without a damping coefficient was used for the analysis (see Table 3). The damping coefficient was omitted as it is negligible for aluminium alloys. Then, the model was discretised, mainly using the finite element 'SOLID185' (see Fig. 13).

After discretisation, the dynamic equation of motion necessary to calculate the frequency and mode of natural vibrations can be written in the following form [24]:

$$M\ddot{u} + C\dot{u} + Ku = p(t) \tag{1}$$

where M, C and K are the global mass, global damping and global stiffness matrices, respectively; $p(t)$ is the time-dependent applied force vector; $\ddot{u}$, $\dot{u}$ and u are the nodal acceleration, nodal velocity and nodal displacement vectors, respectively.

The global mass and damping matrices are assembled from the element matrices that are given by the following equations:

$$M^{(e)} = \int_{V^{(e)}} \rho^{(e)} N^T N \, dV \tag{2}$$

$$C^{(e)} = \int_{V^{(e)}} c_s^{(e)} N^T N \, dV \tag{3}$$

$$K^{(e)} = \int_{V^{(e)}} \rho^{(e)} B^T E B \, dV \tag{4}$$

where $M^{(e)}$, $C^{(e)}$ and $K^{(e)}$ are the element's mass, damping and stiffness matrices; $\rho^{(e)}$ is the density of element 'e'; $V^{(e)}$ – volume of element 'e'; N is the matrix of the element's shape functions; B and E, respectively, are the matrices of the derivatives of the shape functions and the material stiffness.

Omitting the exciting force and damping, we get the final equation, which is used to determine the natural frequency, as follows:

$$\left(K - \omega^2 M\right) \cdot \bar{u} = 0, \tag{5}$$

where ω is the natural frequency (eigenvalue) and $\hat{u}$ is the form of natural vibrations (eigenvector).

Table 3. Material parameters adopted during numerical analysis.

Parameter	Value
Density	2760 kg/m^3
Young's Module	72 GPa
Poisson number	0.32

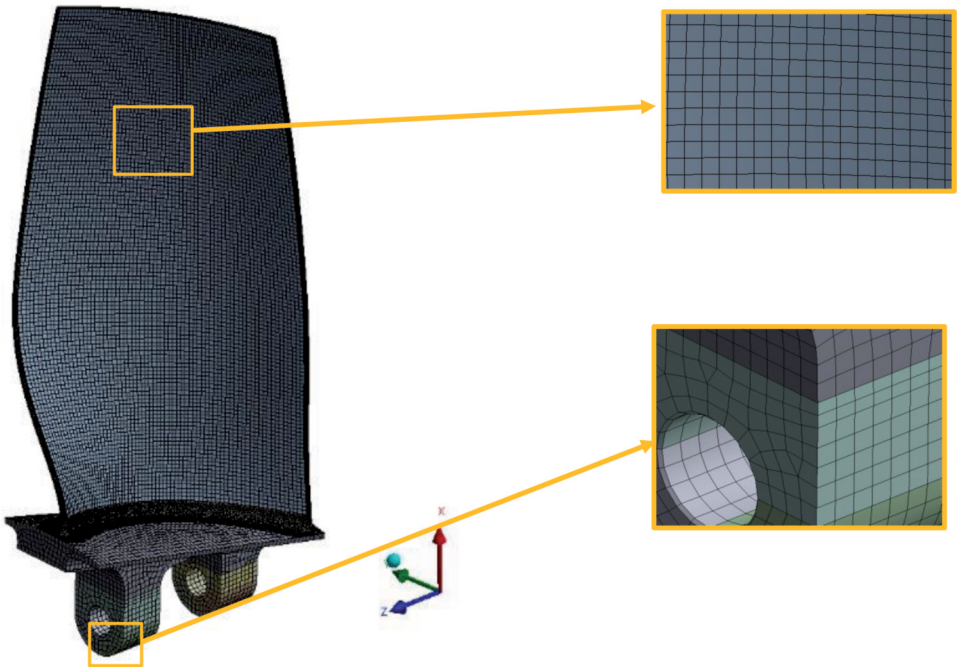

Figure 13. Model of a blade with a mesh type SOLID185; discretisation of the model with finite elements was performed manually.

The analysis was performed for the 'free–free' condition. This means that the tested geometry has no constraints and no external forces. With such a boundary condition, the calculations were performed in the range of 0–2,000 Hz to find all forms of natural vibrations and the frequencies assigned to them.

3.2 Results of the modal analysis

As a result of the numerical analysis, nine frequencies, along with the corresponding mode shapes, were obtained. The first six were not considered. These figures were the result of the motion of a rigid body, and each of them corresponded to a displacement or rotation in relation to one of the axes of the assumed coordinate system. Their frequency values were close to zero.

The results of the remaining three frequencies and vibration modes for the assumed 'free–free' boundary condition are shown in Fig. 14. It is worth mentioning that the 'min–max values' in the legend with the displacement scale were not considered because they do not correspond to real displacements and they are normalised to the mass matrix. Therefore, only the extent of the largest and the smallest displacement observed in each form is shown.

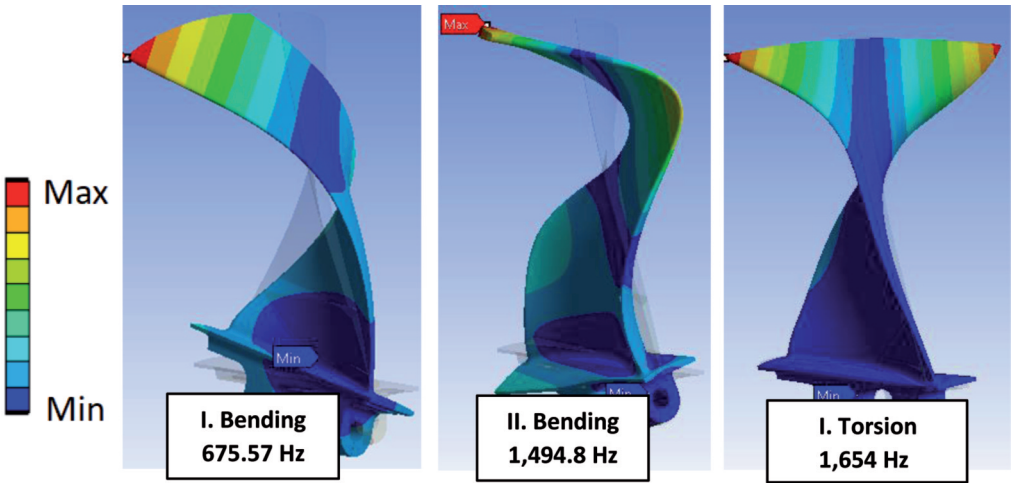

Figure 14. Results of the frequency and mode of free vibrations of the blade obtained by numerical calculations.

4. STATEMENT OF THE RESULTS

Table 4 presents the values of the natural frequencies obtained through tests and numerical analysis. The result obtained from the excitation of blade no. 10 was used as a reference, as its mass was closest to the nominal one (CAD model). For each of the calculated values, the percentage difference that occurred between the experimental and theoretical calculations was determined.

Table 4. List of results of the natural frequencies obtained experimentally and numerically.

	$f1$ 1. Bending	$f2$ 2. Bending	$f3$ 1.Torsion	$f2/f1$	$f3/f1$
Test results	666.625 Hz	1,473.625 Hz	1,635 Hz	2.21	2.45
Numerical analysis results	675.57 Hz	1,494.8 Hz	1,654 Hz	2.21	2.45
Error	1.3%	1.4%	1.2%		

Comparing the simulation results (see Fig. 14) against those identified by the experimental method (see Fig. 5), it can be seen that the numerical model correctly represents the figures observed in the test laboratory.

5. ASSESSMENT OF STRUCTURAL DEFECT RISK

Measurements of the natural frequencies of the tested blades showed differences in each blade. The reason is not the differences in material properties between the tested objects (density and Young's modulus) because they were made of the same raw material. Therefore, it was suspected that the variation in blade geometry or structural defects of each blade (e.g., cracks, porosity and non-metallic inclusions) would credibly explain the frequency variation. Figure 15 shows the frequency probability distribution for the three forms against the background of the theoretical distribution assuming normal distribution checked using the Anderson–Darling method; the Y-axis shows a normal distribution span. Extreme

points designated as 'Anomaly?' have such a large deviation from the average value that it may be questioned whether such a value can result only from differences in the quality of the airfoils.

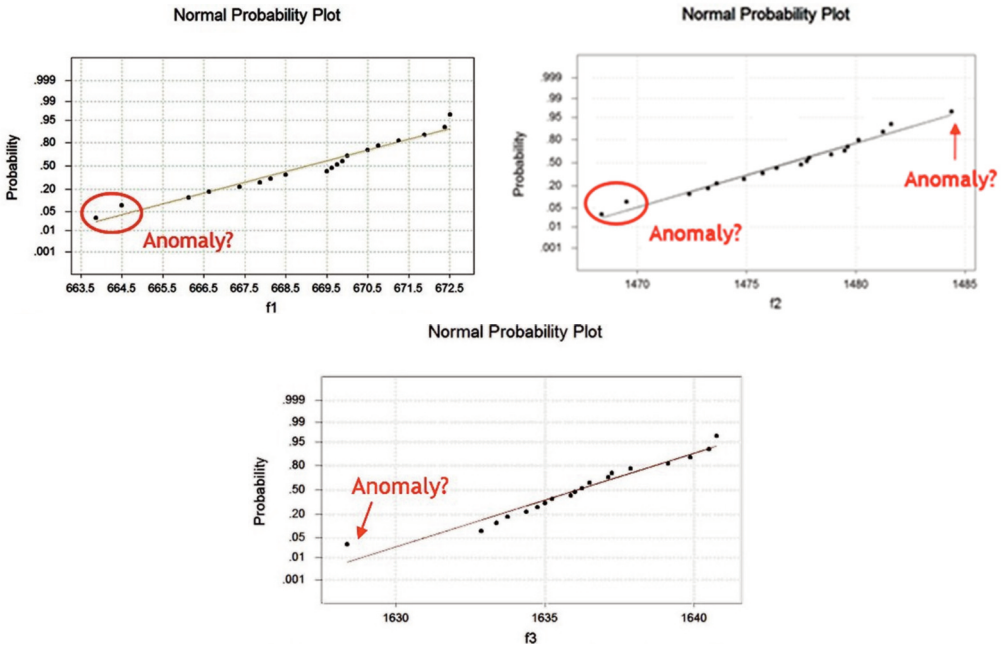

Figure 15. Probability distribution for differences in natural frequencies (dots). The line shows the expected normal distribution for a population of 20 blades.

To determine whether the differences in the weight of the blades translate into differences in frequencies, a blade sensitivity analysis was performed based on a simplified analytical solution. It was assumed as follows:

- During the manufacture of the blade, controlling the machining process in the airfoil area is the most difficult because of its thickness and the type of the material, i.e., low Young's modulus, creating difficulties in maintaining the desired airfoil thickness. Therefore, it was arbitrarily assumed that 75% of the differences in the blades' mass directly translate into a uniform change in the thickness of the blade; the remaining 25% had no effect on vibrations.
- Blade vibration can be simplified in the analytical model, which is a flat rectangular plate of uniform thickness restrained at one edge (thickness corrected for 75% of the blade weight difference). This type of geometry allows for the appearance of similar figures as in the full blade model, i.e., two bent and one torsional forms. The formula to determine the natural frequencies in a plate as defined above is as follows [25]:

$$f_{ij} = \frac{\lambda_{ij}^2}{2 \cdot \pi \cdot a^2} \sqrt{\frac{E \cdot h^2}{12 \cdot \gamma \cdot \left(1 - \upsilon^2\right)}},$$

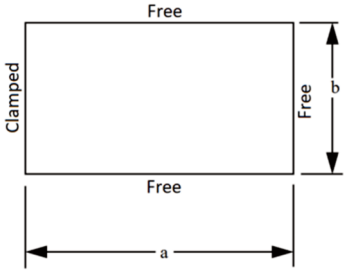

where:

– a is the plate length in the direction perpendicular to the edge of the restraint (blade length);
– h is the plate thickness;
– λ_{ij} is a constant determined from the finite element method (FEM) model or appropriate tables for the selected vibration modes and proportions of the slab dimensions (a/b, where 'b' is the length along the blocked edge, i.e., the blade lock in this case);
– i is the number of half-waves along the length 'a' for the vibration modes (i.e., for this analysis, i = 1 and 2 for both flexural modes);
– j is the number of half-waves along the length 'b' for the vibration mode (i.e., for this analysis j = 0 for both bent forms and j = 1 for the torsional form);
– E is the Young's modulus;
– υ is the Poisson constant;
– γ is the slab mass per unit area, i.e., thickness h multiplied by material density.

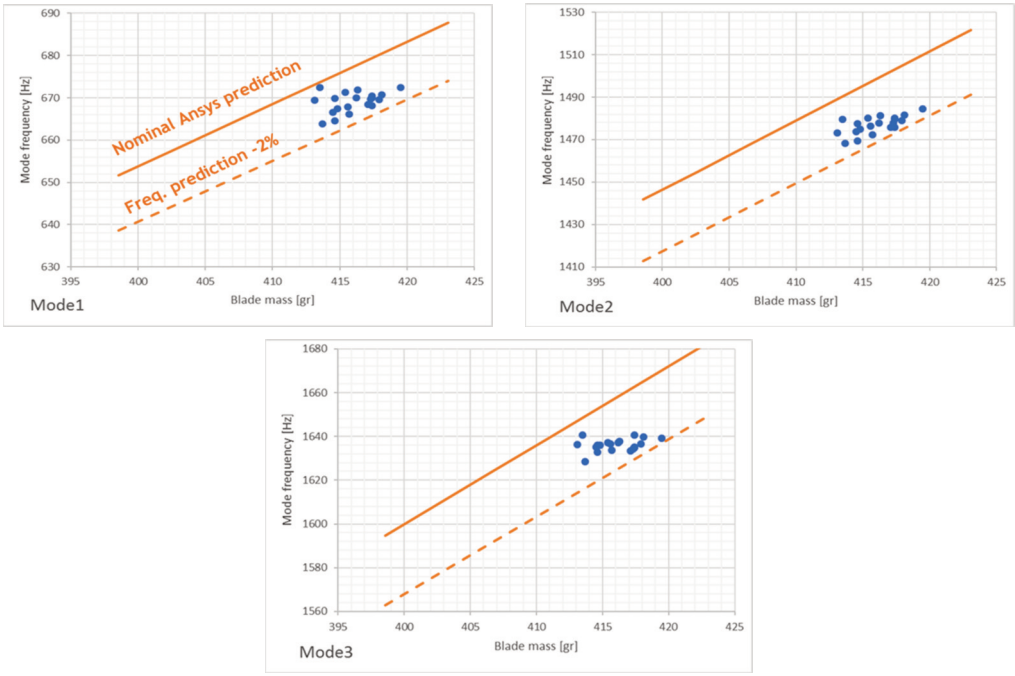

Figure 16. The results of the analytical solution considering the mass of the tested blades using the plate model.

The above analytical solution allows for determination of the change in a blade's frequency in a situation where the variables are different than in the FEM model, without the need to convert the modified blade in FEM analysis. In the above analysis, the coefficients λ_{ij} for the three recognised forms for the conventional values of a, b, h and γ (mean as in the blade model) have been described by the digital model. In the next step, the frequencies f_{ij} were calculated for the plate with nonstandard thickness 'h', where the arbitrary assumption of 75% increase or decrease in the blade mass resulted from the uniform change in its thickness in the airfoil area. The results of the above calculations are shown in the following graphs (see Fig. 14). The solid line of Fig. 16 shows the expected frequencies in the model assuming 75% of the differences in the mass of the blades were to be translated into the blade's thickness. The blue dots are the measured values for the 20 blades. As the result, all of these points deviate

from the analytical model's base line by <2%. Additionally, none of the examined blades differed in the frequency-to-mass proportion from the remaining ones. Therefore, it was concluded that within the tested set of 20 blades, none had any structural defect, and the differences in frequency are related to the normal machining quality of a thin blade in a compliant material such as an aluminium alloy.

6. DETERMINATION OF THE ACTUAL AIRFOIL GEOMETRY BASED ON A MODAL TEST

Since it was found that the blades did not have any structural defect, it was decided to conduct a study to estimate the possible thickness of the airfoil for each of the tested blades. For this purpose, four additional simulations were performed based on previously prepared CAD models. The numerical modal analysis was carried out for two sets of two blades per set. It consisted of two with a thinner blade and two with a blade thickened by 0.1 mm and 0.2 mm over the entire volume. Based on the obtained results, how a change in airfoil thickness—volume—influences the structural stiffness for each of the tested vibration modes was estimated (see Fig. 17).

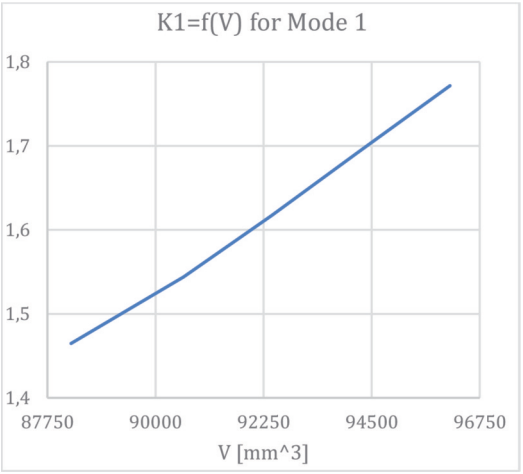

Figure 17. Influence of the airfoil volume on the stiffness *K*1 for the first vibration frequencies (chart shown only for first mode shape).

Based on the knowledge of the weight of blades, an estimation of the volume for each blade was made. By interpolating the results into the Kn f(V) curve, the stiffness was determined, and the vibration frequency was calculated for each of the tested objects. In the worst case, the obtained results differed by 1.9% from the measured values. The result was identical to the one obtained through the analytical calculations. Therefore, the volumes for each blade, whereby the first vibration frequency would give a result identical to the experimental result, were determined. For this purpose and based on the results obtained through laboratory tests, the structural stiffness 'Kn' of each airfoil was determined. By interpolating the obtained values into a previously determined curve, the volume was set, and afterwards, the thickening or thinning was estimated. The results of the study are presented in Table 5.

Table 5. Result of adjusting the airfoil volume to the first natural frequency (negative sign in 'thickening/thinning airfoil' column indicates that the blade has been thinned relative to the nominal geometry).

No. Blade	mass	Thickening /thinning airfoil	Mass of:		The frequency of vibrations based on the determined volume of the airfoil					
			Airfoil	Root	Mode 1	Error	Mode 2	Error	Mode 3	Error
	m [g]	[mm]	m [g]		[Hz]		[Hz]		[Hz]	
3	413.1	-0.0371	251.0	162.1	669.50	0.00%	1,478.84	-0.38%	1,643.53	-0.44%
14	413.5	-0.0205	252.8	160.7	672.50	0.00%	1,485.86	-0.43%	1,648.96	-0.52%
11	413.7	-0.0673	247.6	166.1	663.88	0.00%	1,465.69	0.18%	1,633.36	-0.31%
10	414.5	-0.0527	249.3	165.2	666.63	0.00%	1,472.11	0.10%	1,638.32	-0.20%
2	414.6	-0.0640	248.0	166.6	664.50	0.00%	1,467.13	0.16%	1,634.47	-0.10%
12	414.6	-0.0350	251.2	163.4	669.88	0.00%	1,479.73	-0.15%	1,644.22	-0.51%
6	414.8	-0.0486	249.7	165.1	667.38	0.00%	1,473.88	0.07%	1,639.68	-0.23%
15	415.4	-0.0275	252.1	163.3	671.25	0.00%	1,482.92	-0.19%	1,646.69	-0.58%
7	415.6	-0.0459	250.0	165.6	667.88	0.00%	1,475.05	0.09%	1,640.59	-0.25%
20	415.7	-0.0553	249.0	166.7	666.13	0.00%	1,470.96	0.10%	1,637.43	-0.23%
16	416.2	-0.0344	251.3	164.9	670.00	0.00%	1,480.00	-0.14%	1,644.42	-0.45%
18	416.3	-0.0240	252.5	163.8	671.88	0.00%	1,484.40	-0.21%	1,647.83	-0.61%
1	417.1	-0.0426	250.4	166.7	668.50	0.00%	1,476.49	-0.05%	1,641.71	-0.51%
4	417.3	-0.0357	251.2	166.1	669.75	0.00%	1,479.43	-0.11%	1,643.98	-0.59%
5	417.4	-0.0343	251.3	166.1	670.00	0.00%	1,480.02	-0.03%	1,644.44	-0.56%
13	417.4	-0.0316	251.6	165.8	670.50	0.00%	1,481.19	-0.07%	1,645.34	-0.28%
17	417.4	-0.0446	250.2	167.2	668.13	0.00%	1,475.63	0.01%	1,641.05	-0.39%
9	417.9	-0.0364	251.1	166.8	669.63	0.00%	1,479.14	-0.02%	1,643.76	-0,44%
8	418.1	-0.0302	251.8	166.3	670.75	0.00%	1,481.77	-0.01%	1,645.80	-0.36%
19	419,5	-0,0212	252,8	166,7	672,38	0,00%	1,485,57	-0,08%	1,648,74	-0,59%

7. CONCLUSIONS

This article presents a method aimed at estimating the geometrical properties of rotor blades based on a modal study. The described method consists of adjusting the results obtained by analytical calculations to the results obtained by experimental studies.

The first step in determining the dynamic properties of the tested objects was to describe the form of vibrations in the range of 0–2,000 Hz. For this purpose, one of the blades was equipped with 11 accelerometers and then excited with a modal hammer. As a result, three frequencies with the corresponding forms of vibrations were obtained. In the next step, the vibration frequencies of all 20 blades were determined. Initially, the verification was carried out on two objects and was aimed at comparing the acceleration spectra obtained from the accelerometers with the acoustic response. As the outcomes of the above comparison turned out to be identical, the result for all the remaining blades was recorded using only the microphone. This approach allowed the testing of the object without any additional sensors and wires mounted on the blade surface, thus eliminating elements that could affect the accuracy of the test results.

In the second step, analytical calculations were performed on the blade with the nominal geometry using the ANSYS software. The obtained results were compared with the experimental outcomes. As there was a slight difference between the measured and the calculated frequencies, it was decided to conduct a study to determine what could be the cause of the differences. Based on the analytical calculations, it was found that none of the tested blades had any structural defects. Using numerical models, it was determined how the airfoil geometry would have to change to give the results consistent with respect to the first vibration frequency. The outcome of the study has shown that all blades could have had thinned airfoils in relation to the nominal one. This may be the result of wrongly selected machining process technology. The conclusion of the research is the fact that modal analysis can be used to determine the geometric properties of already-manufactured parts. The above method can be used to check for the possibility of structural defects also, which in the case of blades operating under high fatigue loads would disqualify them from being installed on the aircraft engine.

REFERENCES

[1] Sun, X., Xu, D. and Sun, D. "Recent Development of Casing Treatments for Aeroengine Compressors." *Chinese Journal of Aeronautics* Vol. 32 (2019): pp. 1–36. DOI: 10.1016/j.cja.2018.11.005.

[2] Farid, A.M. and Adnan, Elshafei M. "Finite Element Analysis of Compressor Blades Under Extension, Bending and Torsion Loads." *Proceeding of the 12-th ASAT Conference*, 29–31 May 2007, MTC, Cario. DOI: 10.21608/asat.2007.24386.

[3] Fu, Xi, Ma, Chao, Jiewei Lin and Junhong Zhang. "Numerical Study on Vibration Response and Fatigue Damage of Axial Compressor Blade Considering Aerodynamic Excitation." *Metals* Vol. 11 (2021): p. 1835. DOI: 10.3390/met11111835.

[4] Tsymbalyuk, V. and Linhart, J. Corrections of Aerodynamic Loadings Measurement on Airfoil Cascade at Bending Torsion Vibrations – XVII IMEKO Congress, Dubrovnik, Croatia, pp. 358-361, June 22-27, 2003.

[5] Zbigniew, L. Kowalewski – Zmęczenie Materiałów – Podstawy, Kierunki Badań, Ocena Stanu Uszkodzenia, XVII Seminarium Nieniszczące Badania Materiałów, Zakopane (8-11 marca 2011).

[6] Witoś, Mirosław. "Zwiększenie żywotności silników turbinowych poprzez aktywne diagnozowanie i sterowanie." *Prace Naukowe Instytutu Technicznego Wojsk Lotniczych*, (2011); nr 29: pp. 3–324.

[7] Tommy J. George, Herman Shen, M.H., Onome Scott-Emuakpor, Theodore Nicholas, Charles J. Cross and Jeffrey Calcaterra. "Goodman Diagram Via Vibration-Based Fatigue Testing." *Journal of Engineering Materials and Technology* Vol. 129 (2005): pp. 58–64. DOI: 10.1115/1.1836791.

[8] Natke, H.G. and Cempel, C. "Model Aided Diagnosis Based on Symptoms." International Conference on Damage Assessment of Structures J. M. Dulieu-Smith W. J. Staszewski and K. Worden. 1997. *Structural Damage Assessment Using Advanced Signal Processing Procedures: Proceedings of DAMAS '97*, University of Sheffield, UK, pp. 363–375, 30 June-2 July 1997. Sheffield Academic Press.

[9] Lay Menn Khoo, P. Raju Mantena and Prakash Jadhav. "Structural Damage Assessment Using Vibration Modal Analysis." *Structural Health Monitoring* Vol. 3 (2004): p. 177. DOI: 10.1177/1475921704042680.

[10] Zimmerman, D.C., Smith, S.W., Kim, H.M. and Bartkowicz, T.J. "Spacecraft Applications for Damage Detection Using Vibration Testing." *Proceedings of the 14th International Modal Analysis Conference* Vol. 1 (1996): pp. 851–856.

[11] Witoś, Mirosław. "On the Modal Analysis of A Cracking Compressor Blade." *Research Works of Air Force Institute of Technology* No. 23 (2008): pp. 21–36. DOI: 10.2478/v10041-008-0016-0.

[12] Jerzy Madej, Marek Sitek. "Analiza Modalna i Harmoniczna Modelu Zespołu Elektrowibratora Przy Różnej Konfiguracji Ciężarów." *Acta Mechanica et Automatica* Vol. 5, No. 3 (2011): 87–90.

[13] Wiesław Krzymień. "Identyfikacja nieliniowych drgań konstrukcji lotniczych." Seria Monograficzna: Biblioteka Naukowa Instytutu Lotnictwa, nr 58, (2019). ISBN 978-83-63539-52-8.

[14] Gloth, G. and Sinapius, M. Analysis of Swept-Sine Runs During Modal Identification." *Mechanical Systems and Signal Processing* (2004); 18 (6): pp. 1421–1441. DOI: 10.1016/S0888-3270(03)00087-6.

[15] Tadeusz Uhl. "Zastosowanie analizy modalnej w diagnostyce maszyn." *Diagnostyka* Vol. 23 (2000): pp. 82–87.

[16] Matsuo M., Yasui T., Inamura T. and Matsumura M. "High-Speed Test of Thermal Effects for a Machine-tool Structure Based on Modal Analysis." *Precision Engineering* (1986); 8 (2): pp. 72–78. DOI: 10.1016/0141-6359(86)90089-9.

[17] Li, Bin, Cai, Hiu, Mao, Xinyong, Huang, Junbin and Luo, Bo "Estimation of CNC Machine-tool Dynamic Parameters Based on Random Cutting Excitation Through Operational Modal Analysis." *International Journal of Machine Tools & Manufacture* (2013) 71: pp. 26–40. DOI: 10.1016/j.ijmachtools.2013.04.001.

[18] Zaghbani, I. and Songmene, V. "Estimation of Machine-tool Dynamic Parameters During Machining Operation Through Operational Modal Analysis." International Journal of Machine Tools & Manufacture (2009), 49 (12-13): pp. 947–957. DOI: 10.1016/j.ijmachtools.2009.06.010.

[19] Zhang, G.P., Huang, Y.M., Shi, W.H. and Fu, W.P. "Predicting Dynamic Behaviors of a Whole Machine Tool Structure Based on Computer-aided Engineering." *International Journal of Machine Tools & Manufacture* (2003); 43 (7): pp. 699–706. DOI: 10.1016/S0890-6955(03)00026-9.

[20] Gagnol, V., Le, T.P. and Ray, P. "Modal Identification of Spindle-tool Unit in High-speed Machining." *Mechanical Systems and Signal Processing* (2011); 25 (7): pp. 2388–2398. DOI:10.1016/j.ymssp.2011.02.019.

[21] Vivo, A., Brutti, C. and Leofanti, J. "Modal Shape Identification of Large Structure Exposed to Wind Excitation by Operational Modal Analysis Technique." *Mechanical Systems and Signal Processing* (2013); 39 (1-2) pp. 195–206. DOI: 10.1016/j.ymssp.2013.03.025.

[22] Rahmatalla, S., Hudson, K., Liu, Y. and Eun, H.Ch. "Finite Element Modal Analysis and Vibration-waveforms in Health Inspection of Old Bridges." *Finite Elements in Analysis and Design* (2014); 78: pp. 40–46. DOI: 10.1016/j.finel.2013.09.006.

[23] Maria Virginia Gelfuso, Daniel Thomazini, Júlio César Silva de Souza and José Juliano de Lima Junior. "Vibrational Analysis of Coconut Fiber-PP." *Composites. Materials Research* 2014, 17 (2), 367–372. DOI: http://dx.doi.org/10.1590/S1516-14392013005000200.

[24] de Silva, C. *Vibration and Shock Handbook*. Taylor & Francis, Boca Raton (2005).

[25] "Modal Analysis of a Flat Plate" Available at: https://www.yumpu.com/en/document/read/24181727/1-modal-analysis-of-a-flat-plate-scc.